The Geological Society of America
Special Paper 505
2014

Atmospheric halogen and acid rains during the main phase of Deccan eruptions: Magnetic and mineral evidence

Eric Font*
Instituto Dom Luís, Faculdade de Ciências, Universidade de Lisboa (IDL-FCUL), Edifício C8-8.3.22, Campo Grande, 1749-016, Portugal

Sébastien Fabre
Institut de Recherche en Astrophysique et Planétologie (IRAP), Observatoire Midi-Pyrénées (OMP), Université de Toulouse, 31028 Toulouse 24 Cedex 4, France

Anne Nédélec
Géosciences Environnement Toulouse (GET), UMR 5563, Université de Toulouse, 31400 Toulouse, France

Thierry Adatte
Earth Sciences Institute (ISTE), Université de Lausanne, Geopolis, CH-1015 Lausanne, Switzerland

Gerta Keller
Geosciences Department, Princeton University, Princeton, New Jersey 08544, USA

Cristina Veiga-Pires
Centro de Investigação Marinha e Ambiental (CIMA), Faculdade de Ciencias e Tecnologia, Universidade do Algarve, Campus de Gambelas, 8005-139 Faro, Portugal

Jorge Ponte
Instituto Dom Luís, Universidade de Lisboa (IDL-UL), Edifício C8-8.3.22, Campo Grande, 1749-016, Portugal

José Mirão
HERCULES Laboratory (HERança CULtural Estudos e Salvaguarda/Cultural Heritage Studies and Safeguard), University of Evora, 7000-809 Evora, Portugal

Hassan Khozyem
Earth Sciences Institute (ISTE), Université de Lausanne, Geopolis, CH-1015 Lausanne, Switzerland and *Geology Department, Faculty of Sciences, Aswan University, 81528-Aswan, Egypt*

Jorge E. Spangenberg
Institute of Earth Surface Dynamics (IDYST), University of Lausanne, Building Géopolis, CH-1015 Lausanne, Switzerland

*font_eric@hotmail.com

Font, E., Fabre, S., Nédélec, A., Adatte, T., Keller, G., Veiga-Pires, C., Ponte, J., Mirão, J., Khozyem, H., and Spangenberg, J., 2014, Atmospheric halogen and acid rains during the main phase of Deccan eruptions: Magnetic and mineral evidence, *in* Keller, G., and Kerr, A.C., eds., Volcanism, Impacts, and Mass Extinctions: Causes and Effects: Geological Society of America Special Paper 505, p. 353–368, doi:10.1130/2014.2505(18).

ABSTRACT

Environmental changes linked to Deccan volcanism are still poorly known. A major limitation resides in the paucity of direct Deccan volcanism markers and in the geologically short interval where both impact and volcanism occurred, making it hard to evaluate their contributions to the mass extinction. We investigated the low-magnetic-susceptibility interval just below the iridium-rich layer of the Bidart (France) section, which was recently hypothesized to be the result of paleoenvironmental perturbations linked to paroxysmal Deccan phase 2. Results show a drastic decrease of detrital magnetite and presence of scarce akaganeite, a hypothesized reaction product formed in the aerosols derived from reaction of a volcanic plume with water and oxygen in the high atmosphere. A weathering model of the consequences of acidic rains on a continental regolith reveals nearly complete magnetite dissolution after ~31,000 yr, which is consistent with our magnetic data and falls within the duration of the Deccan phase 2. These results highlight the nature and importance of the Deccan-related environmental changes leading up to the end-Cretaceous mass extinction.

INTRODUCTION

The history of Earth is punctuated by five severe global climatic and environmental catastrophes that led to nearly total mass extinctions of calcareous marine and many continental species. The most famous case is the Cretaceous-Paleogene boundary (KPB or Cretaceous-Tertiary boundary [KTB]) mass extinction, which is still the center of acrimonious debates between partisans of the bolide impact theory (Schulte et al., 2010) and those who favor a terrestrial origin linked to Deccan Traps volcanism (Courtillot, 2012; Keller et al., 2012). Others argue that each process, individually, is unlikely to have caused a global biological collapse, and a scenario of multiple causes is preferred (White and Saunders, 2005; Keller et al., 2009; Renne et al., 2013).

In recent years, Deccan volcanism studies have resulted in major advances that now facilitate recognition and evaluation of its global effects, such as attempted in this study. For example, three discrete Deccan volcanism phases with variable intensity have been dated based on magnetostratigraphy and ^{40}K-^{40}Ar ages (Chenet et al., 2007): Phase 1 in the early late Maastrichtian (base magnetozone C30n, ca. 67.4 Ma) accounts for ~6% of the total lava pile, which today forms mountain peaks of 3500 m (Self et al., 2006). Most of the lava pile (80%) erupted during phase 2 in the latest Maastrichtian paleomagnetic chron C29r. The final phase 3 erupted in the early Danian base of C29n and accounts for ~14% of total Deccan eruptions (Chenet et al., 2007, 2008; Keller et al., 2011, 2012). The original size prior to erosion is estimated to have been 1.5×10^6 km^2, and the volume of lava extruded is estimated at ~1×10^6 km^3 (Self et al., 2006; Chenet et al., 2007).

Most critical for the current study is Deccan volcanism phase 2, which has been directly linked to the Cretaceous-Paleogene boundary mass extinction in outcrops and deep wells of the Krishna-Godavari Basin in India (Keller et al., 2011, 2012). These studies revealed Earth's longest lava megaflows (Self et al., 2008a), 1500 km across India near the end of phase 2, with the final megaflow at the Cretaceous-Paleogene boundary mass extinction (Keller et al., 2008).

Current research thus narrows the main phase 2 of Deccan volcanism to the geologically short interval of the Cretaceous planktic foraminiferal zone CF1, which spans the last ~160,000 yr below to the Cretaceous-Paleogene boundary, whereas the Chicxulub impact is commonly placed at the Cretaceous-Paleogene boundary (Schulte et al., 2010) or within zone CF1 preceding the mass extinction (Keller et al., 2012). This short interval limits our ability to separate the main Deccan volcanic phase (i.e., phase 2) from the Chicxulub impact within resolvable radiometric ages and to evaluate their respective biotic effects and their contributions to the Cretaceous-Paleogene boundary mass extinction. Radiometric (K-Ar and Ar-Ar) methods are subject to intrinsic errors (~1%–2%), linked to interlaboratory calibration, imprecise K and Ar isotopic standards (Fish Canyon standard), and uncertainty of decay constants (Kuiper et al., 2008; Channell et al., 2010; Renne et al., 2010, 2013), preventing any precise radiometric age correlation between continental Deccan flood basalts and the mass extinction recorded in marine sections. In addition, because volcanic mineralogical markers (aerosols) are generally restricted to the vicinity of the volcanic source, the discrimination between Deccan phase 2 and the Chicxulub impact in distal sections is even harder within such a short temporal interval.

Are volcanic signals present but unrecognized outside India? A recent study of Cretaceous-Paleogene boundary sections at Bidart, France, and Gubbio, Italy, suggests so (Font et al., 2011). In these sections, a 50-cm-thick yellow-red interval of very low magnetic susceptibility (MS) directly underlies the Cretaceous-Paleogene boundary (Fig. 1), as also observed in Oman (Ellwood et al., 2003) and other marine sections. Preliminary data indicate that this low-MS interval contains an enigmatic Cl-rich iron oxyhydroxide that could have formed by

interaction between HCl-rich volcanic gas and aerosols in the high atmosphere (Font et al., 2011). The plate-like morphology and well-preserved texture of this newly discovered mineral strongly contrast with the detrital aspect of titanomagnetite and suggest an eolian origin for its transport. Recent numerical modeling showed that penetrative convection driven by the cooling of the Deccan lavas may have generated buoyant atmospheric plumes (Kaminski et al., 2011). In such a situation, aerosols would have been able to rise to the stratosphere, providing an explanation for a rather long halogen residence time in the atmosphere and the eventual transport of their reaction products to Bidart and Gubbio sections.

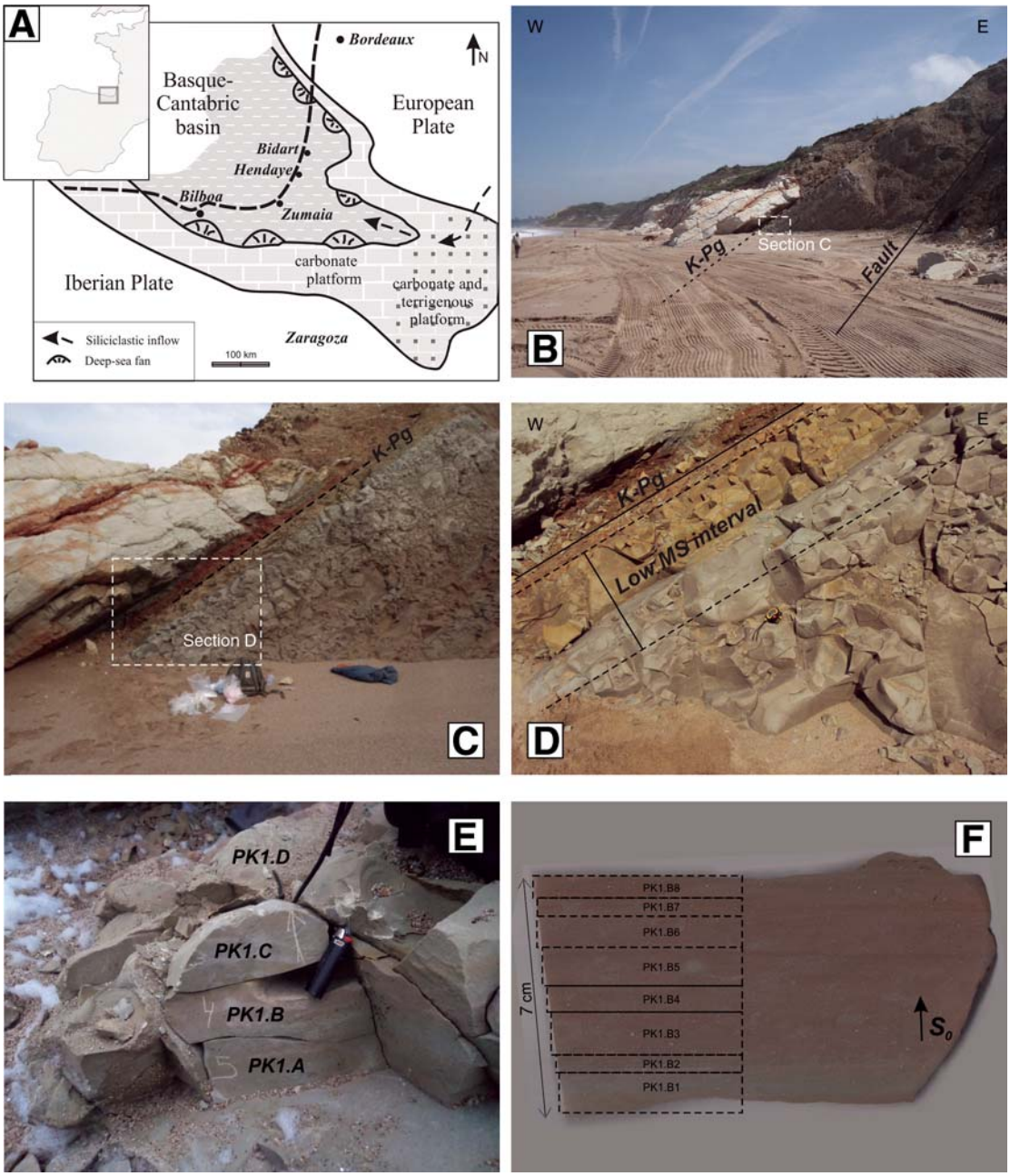

Figure 1. Geological settings and biostratigraphy of the Bidart section. (A) Paleoenvironmental context of the Biscay Bay. (B) The Erretegia Beach showing the white-pink Danian limestones and the Maastrichtian marls cut by a fault. (C) The Cretaceous-Paleogene (K-Pg) boundary showing (D) the typical dark clay layer and the yellow-red interval of low magnetic susceptibility (MS) values in the upper Maastrichtian. (E) Example of hand block collected at the outcrop. (F) Example of a block cut into small plates, by using a nonmagnetic Dremel saw, for subsequent magnetic analyses.

The main objective of this study was to evaluate the magnetic and mineralogical characteristics of the uppermost Maastrichtian at Bidart, France, in order to determine the potential signature of Deccan volcanism. To achieve this objective, the following evaluations were performed: (1) Determine the presence of zone CF1 (latest Maastrichtian correlative with Deccan phase 2) based on high-resolution biostratigraphy and chemostratigraphy (carbon and oxygen isotopes). (2) Perform high-resolution (centimeter-scale) magnetic analyses and microscope observations focused on the last meter of the Maastrichtian, including the low-MS interval, to determine its mineral content and origin. (3) Identify the enigmatic Cl-bearing iron oxyhydroxide and evaluate its possible formation and subsequent transport in relation with the Deccan volcanism. (4) Quantify the effects of acid rains on a continental regolith using a numerical weathering model.

METHODS

For biostratigraphic and faunal analyses, samples were processed using standard methods (Keller et al., 1995). Samples were washed through 38 µm and 63 µm sieves and oven dried at 50 °C. Species preservation is generally good, though shells are recrystallized and affected by dissolution. Dissolution effects are apparent below the Cretaceous-Paleogene boundary coincident with the low-MS interval and a major increase in benthic species. In the 25 cm below the Cretaceous-Paleogene boundary, almost all carbonate shells are dissolved due to intense dissolution. Faunal analysis was conducted on three size fractions (38–63 µm, 63–150 µm, >150 µm) with the quantitative analysis based on 38–63 µm and 63–150 µm size fractions.

We measured MS, saturation isothermal remanent magnetization (SIRM), and coercivity-dependent magnetic properties (e.g., $IRM_{-0.3T}/IRM_1$ = S-ratio, mean acquisition field [$B_{1/2}$]). Mass-specific MS is mainly controlled by ferromagnetic (i.e., iron oxide) and paramagnetic (i.e., clay) contents, whereas isothermal remanent magnetization (IRM) is mostly sensitive to ferro/ferrimagnetic and antiferromagnetic particles, even in very low amounts. MS was measured with a MFK1 (AGICO) apparatus at the Institute Dom Luís Laboratory (Portugal) and reported relative to mass-specific m^3/kg by dividing by density. Samples were cleaned by alternating fields (AF) treatment and submitted to IRM measurements using an impulse magnetizer (IM-10–30). IRM curves were then analyzed using a cumulative log-Gaussian function (Kruiver et al., 2001) in order to discriminate magnetic phases by their respective coercivity spectra. IRM data are normalized by the mass (unit in Am^2/kg) with a constant volume of 10 cm^3. Fresh rock fragments were also observed under a Hitachi S-3700N scanning electron microscope (SEM) coupled to a Bruker XFlash® 5010 energy dispersive spectra (EDS) detector at the Hercules Laboratory (Evora, Portugal). EDS provides semiquantitative compositional analysis.

We also measured the color by using diffuse reflectance spectrophotometry (DRS) analysis, which is based on the percentage reflectance of a sample relative to white light and provides qualitative information about mineralogical and grain-size variations. DRS data were converted into a color by using the Munsell Color System and are represented in L*a*b* coordinates following the Commission International de l'Éclairage (CIE, 1976), where L* is the lightness/darkness, a* is the redness/greenness, and b* is the yellowness/blueness. Data were obtained using a X-Rite® Colortron™ spectrophotometer from 86 rock powders, in order to avoid grain-size effects, and after three series of measurements.

Isotopic analyses were performed at the University of Lausanne on a Thermo Fisher Scientific (Bremen, Germany) GasBench II carbonate preparation device connected to a Thermo Fisher Scientific Delta Plus XL continuous-flow isotope ratio mass spectrometer (IRMS). CO_2 was extracted at 70 °C. Isotopic ratios of carbon and oxygen are reported in the delta (δ) notation as the per mil (‰) deviation relative to the Vienna Peedee belemnite standard (VPDB). The analytical reproducibility estimated from replicate analyses of the international calcite standard NBS-19 and the laboratory standards of Carrara marble was better than ±0.05‰ for $\delta^{13}C_{carb}$ and ±0.1‰ for $\delta^{18}O_{carb}$.

In order to discuss the origin of the loss in detrital magnetite just below the Cretaceous-Paleogene boundary, we processed a numerical weathering model. We used the PHREEQC program (Parkhurst and Appelo, 1999) developed by the U.S. Geological Survey for modeling water-rock interactions, coupled with the Lawrence Livermore National Laboratory database. The program determines the chemical speciation of aqueous solutes and the fugacities of gases, and it attributes each component of the solution to stable aqueous species. It also calculates the activity coefficients of water and the aqueous species, as well as the saturation index of the solution with respect to all the solid phases of the database. The weathered "rock" material is a monolithologic sandy regolith, assumed to have the same mineral composition as the mean continental upper crust (or typical granodiorite) and forming a layer subjected to drainage conditions and reacting with rainwater initially equilibrated with volcanic gases.

In our hypothesis, the initial magnetic particles accumulate from the parent rock during pedogenesis. The regolith alteration is assumed to proceed by a continuous batch process in water-saturated sediment, where the pore water is being periodically replaced by an equivalent volume of fresh rainwater at each rain event (Fabre et al., 2011; Fabre and Berger, 2012). The surface percentage of magnetite is taken equal to 1.8% (Table 1). The mineral reactive surface (*A*) is calculated according a simple parametric law assumed to be a correct approximation of the solid Brunauer-Emmet-Teller (BET) surface (i.e., method of adsorbing-desorbing gases at the mineral surface in order to measure the surface area; Brunauer et al., 1938; Sverdrup and Warfvinge, 1995):

$$A = (8.0x_{clay} + 2.2x_{silt} + 0.3x_{sand} + 0.0x_{coarse})\rho, \quad (1)$$

where x_{clay}, x_{silt}, x_{sand}, and x_{coarse} represent fractions of clay, silt, sand, and coarse materials in the sandy regolith, and ρ is the

TABLE 1. RATE DISSOLUTION CONSTANTS OF SILICATE (FABRE ET AL., 2011) AND MAGNETITE (WHITE ET AL., 1994)

Granodiorite		Sandy regolith
Silicates	% of mineral surface	k_o (T = 20 °C) in mole Si m^{-2} s^{-1}
Quartz	29.9	3.16E–12
Albite	29.9	9.49E–12
Anorthite	22.8	6.32E–12
Orthose	15.6	9.49E–12
Oxides	% of mineral surface	k_o (T = 20 °C) in mole Fe m^{-2} s^{-1}
Magnetite (pH = 3.3)		5.01E–10
Magnetite (pH = 4.3)	1.8	2.39E–10
Magnetite (pH = 5.6)		1.30E–10

regolith density in g/m^3. Other relevant characteristics of the regolith are reported in Table 2.

The rain frequency is linked to the presumed Maastrichtian climate, namely, tropical hot and humid. The runoff is taken as equal to present-day values: 11 L s^{-1} km^2 (Gaillardet et al., 1999). Numerous studies of current conditions indicate the potential role of acidic rainwater in the mobilization of metals (Floor et al., 2011). In this study, we assumed a pH between 3.3 and 4.3, which is typical of rainwater resulting from the mixing between volcanic plumes and atmospheric aerosols (Chudaeva et al., 2006; Calabrese et al., 2011; Floor et al., 2011). These values were measured in the neighborhood of active volcanoes such as Mount Etna. After each rain event, magnetite and rainwater react to reach equilibrium. The overall dissolution rate of the minerals, R_k, considered as a first-order law, is equal to:

$$R_k = \left(\frac{dn}{dt} \right) = k_o A S_w \left(1 - \frac{Q}{K_k} \right) \quad (2)$$

where R_k stands for bulk dissolution rate of mineral k, k_o is the dissolution rate constant in mol m^{-2} s^{-1}, A is the reactive surface area of the solid (m^2/m^3), S_w is the soil moisture (fixed at 30% as a mean value; Sverdrup and Warfvinge, 1995), and Q/K is the saturation ratio. Thermodynamic constants are taken from Fabre et al. (2011) and White et al. (1994). No specific precipitation law was imposed for secondary phases, assuming that secondary phase formation is controlled by the dissolution of source minerals. Moreover, we assumed that the reaction is not controlled by the diffusion through the oxide layer as observed in closed reactors (White et al., 1994). The amount of dissolved magnetite in moles is calculated during each increment. The final value is the time required to dissolve a significant percentage of the initial magnetite mass (90%) corresponding to the observed MS decrease.

AGE AND CORRELATION WITH DECCAN PHASE 2

The Bidart section is generally considered as one of the most complete Cretaceous-Paleogene boundary sections worldwide because of a thin clay layer and Ir anomaly (Bonté et al., 1984; Ward and Kennedy, 1993; Vonhof and Smit, 1997; Galbrun and Gardin, 2004). However, in previous studies, the zone CF1 index species was not observed, leaving doubt as to the presence of a complete sediment record below the Cretaceous-Paleogene boundary. In this study, the zone CF1 index species (*Plummerita hantkeninoides*) was observed, confirming the presence of the correlative interval with Deccan phase 2.

A second independent test for the presence of the uppermost Maastrichtian can be obtained from oxygen and carbon isotopes, and more specifically the global climate warming, which begins in zone CF2 and continues into the lower part of CF1 and the subsequent cooling prior to the Cretaceous-Paleogene boundary (Fig. 2; Li and Keller, 1998; Stuben et al., 2003; Wilf et al., 2003; Abramovich et al., 2010). We measured carbon and oxygen isotope compositions for the entire section (~6 m) at 20 cm intervals, as well as at higher resolution (5 cm intervals) for the low-MS interval of the top 1 m, with comparable results (Figs. 2–3; Table 1). These data show the climate warming beginning in zone CF2 and proceeding into CF1, followed by cooling correlative with South Atlantic Site 525 (Fig. 2). Note that zones CF2 and CF1 span the last 160 and 120 k.y. at the end of the Maastrichtian, respectively. This study thus demonstrates the presence of the latest Maastrichtian at Bidart correlative with Deccan phase 2.

In this study, we hypothesize that Deccan volcanism caused acid rain and ocean acidification. If this is the case, then it should be reflected in the calcareous shells of planktic foraminifera and more specifically by the loss of dissolution-prone thin-walled species. We observed increasing dissolution effects in planktic foraminifera at the Bidart section in the 50 cm below the Cretaceous-Paleogene

TABLE 2. PHYSICAL PROPERTIES OF SANDY REGOLITH

Property	For 1 m^3 parcel
Density of regolith (kg m^{-3})	2.7
Thickness of soil (m)	0.32
Porosity (%)	20
Reactive surface (g m^{-3})	1,600,000
Runoff (L s^{-1} km^{-2})	11

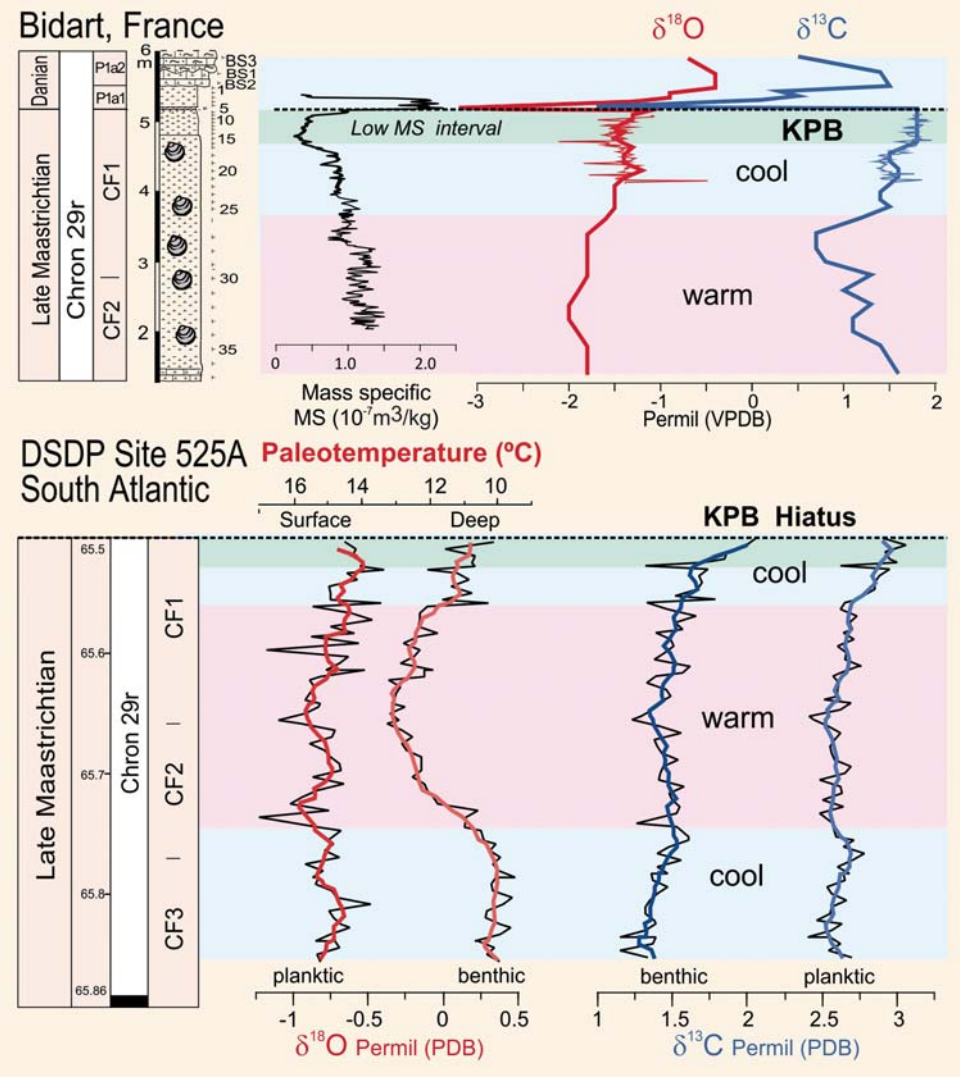

Figure 2. Carbon and oxygen isotopic compositions of the Bidart section and correlation with the South Atlantic (Deep Sea Drilling Project [DSDP] Site 525A; Li and Keller, 1998). The mass-specific magnetic susceptibility (MS) profiles compiled from Font et al. (2011) and the present study are also shown. KPB—Cretaceous-Paleogene boundary; VPDB—Vienna Peedee belemnite.

boundary and correlative with the low-MS interval, with maximum dissolution effects (nearly all species dissolved) in the 20 cm below the Cretaceous-Paleogene boundary (Fig. 2). Increased carbonate dissolution below the Cretaceous-Paleogene boundary has been observed in many sequences (e.g., Smit, 1990; Pardo et al., 1996), but no systematic recording is available to date because the cause has remained unknown. Only recently has Deccan volcanism been identified as a potential cause.

MAGNETIC DATA

The Bidart section was sampled at 1 cm intervals to determine the magnetic properties in the last meter of the Maastrichtian marls (Figs. 1E–1F). Our new high-resolution mass-specific MS analyses confirm the presence of the low-MS interval from –5 to –50 cm below the Cretaceous-Paleogene boundary (Fig. 3). The transition to the more characteristic MS values of the Maastrichtian marls at the base of the interval is gradual, suggesting a progressive change in paleoenvironmental conditions rather than the existence of a hiatus or a fault.

IRM curves show that the main magnetic carrier of the Danian limestones is a low-coercivity phase identified under SEM microscope as detrital titanomagnetite (Fig. 4A). The Danian dark clay layer and the Maastrichtian marls located below the low-MS interval are characterized by a bimodal association (low to high) of coercivity spectra (magnetite and hematite/goethite), whereas the high-coercivity phase alone characterizes the low-MS interval (Fig. 4A). After unmixing raw IRM curves by using the cumulative Log-Gaussian (CLG) function (Robertson and France, 1994; Kruiver et al., 2001), two to three magnetic phases (called components) were isolated (Fig. 4B). Components 1 and 2 correspond to low- to medium-coercivity phases with values of mean acquisition field ($B_{1/2}$) varying from 24 to 80 mT and 57 to 77 mT, respectively (Fig. 4B). CLG parameters of component 1 are in the range of magnetite and maghemite populations commonly found in sedimentary rocks (Kruiver et al.,

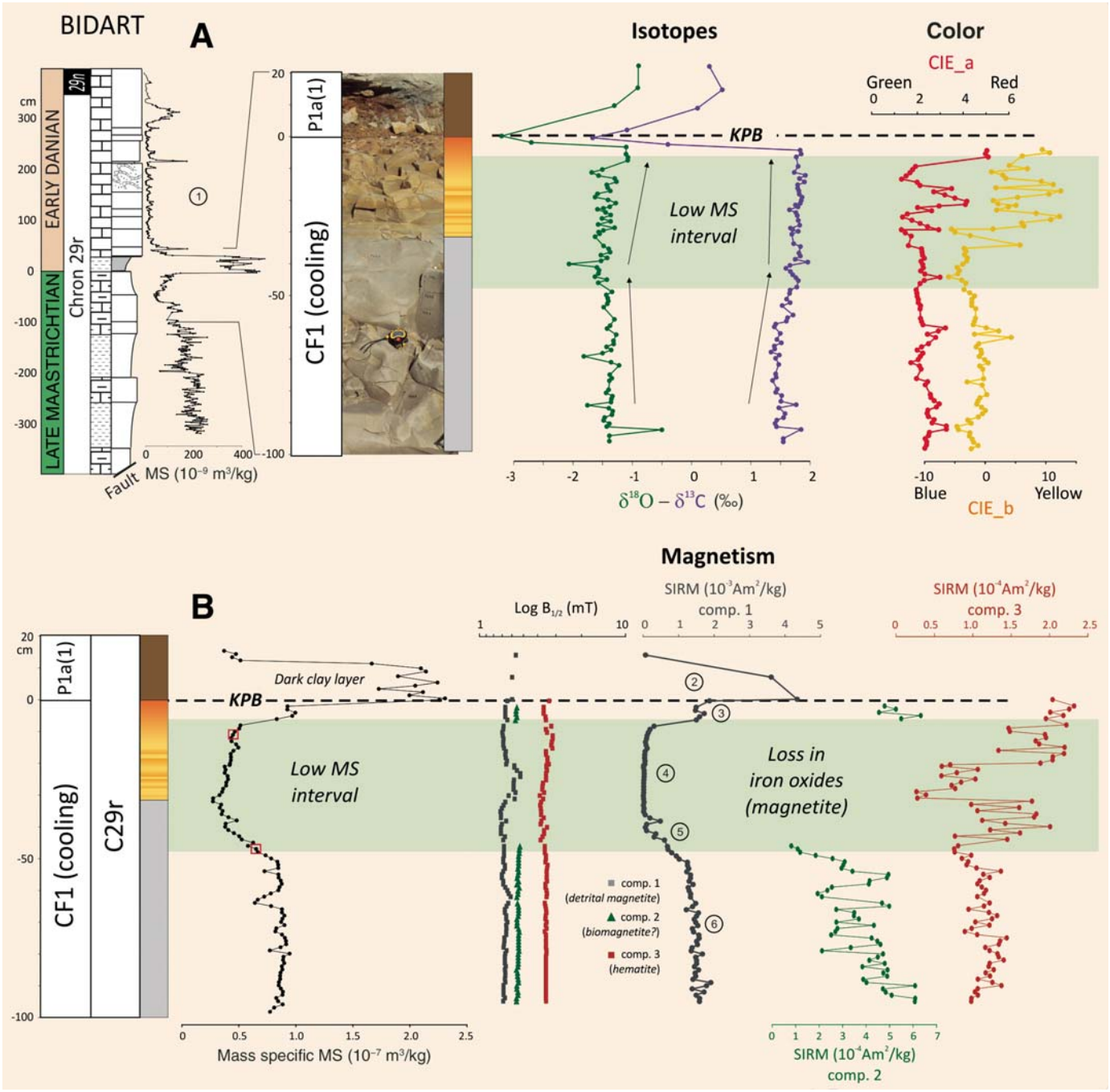

Figure 3. (Top) Magnetic susceptibility (Font et al., 2011; this study) and color profiles along with carbon and oxygen isotope data of the Maastrichtian outcrop at Bidart above the fault line. Carbon and oxygen isotopes mark the climate cooling of the uppermost zone CF1 (see Fig. 2). Diffuse reflectance spectrophotometry shows an increase in red-yellow–colored iron oxides (i.e., akaganeite) in the interval of low-magnetic-susceptibility (MS) values. (Bottom) High-resolution mass-specific MS and isothermal remanent magnetization (IRM) parameters (mean acquisition field [$B_{1/2}$], saturation isothermal remanent magnetization [SIRM]) of the last meter of Maastrichtian marls and the Cretaceous-Paleogene boundary (KPB). The Maastrichtian marls are marked by three magnetic phases (components 1, 2, and 3) assigned to detrital magnetite, biogenic magnetite, and hematite, respectively. The low-MS interval with akaganeite shows a loss in low- to medium-coercivity magnetic phases (components 1 and 2). Red squares on the MS profile show samples analyzed by scanning electron microscopy coupled to energy dispersive spectra (SEM-EDS) and illustrated in Figure 5. Numbered intervals (from 1 to 6) refer to IRM data (shown in Fig. 4).

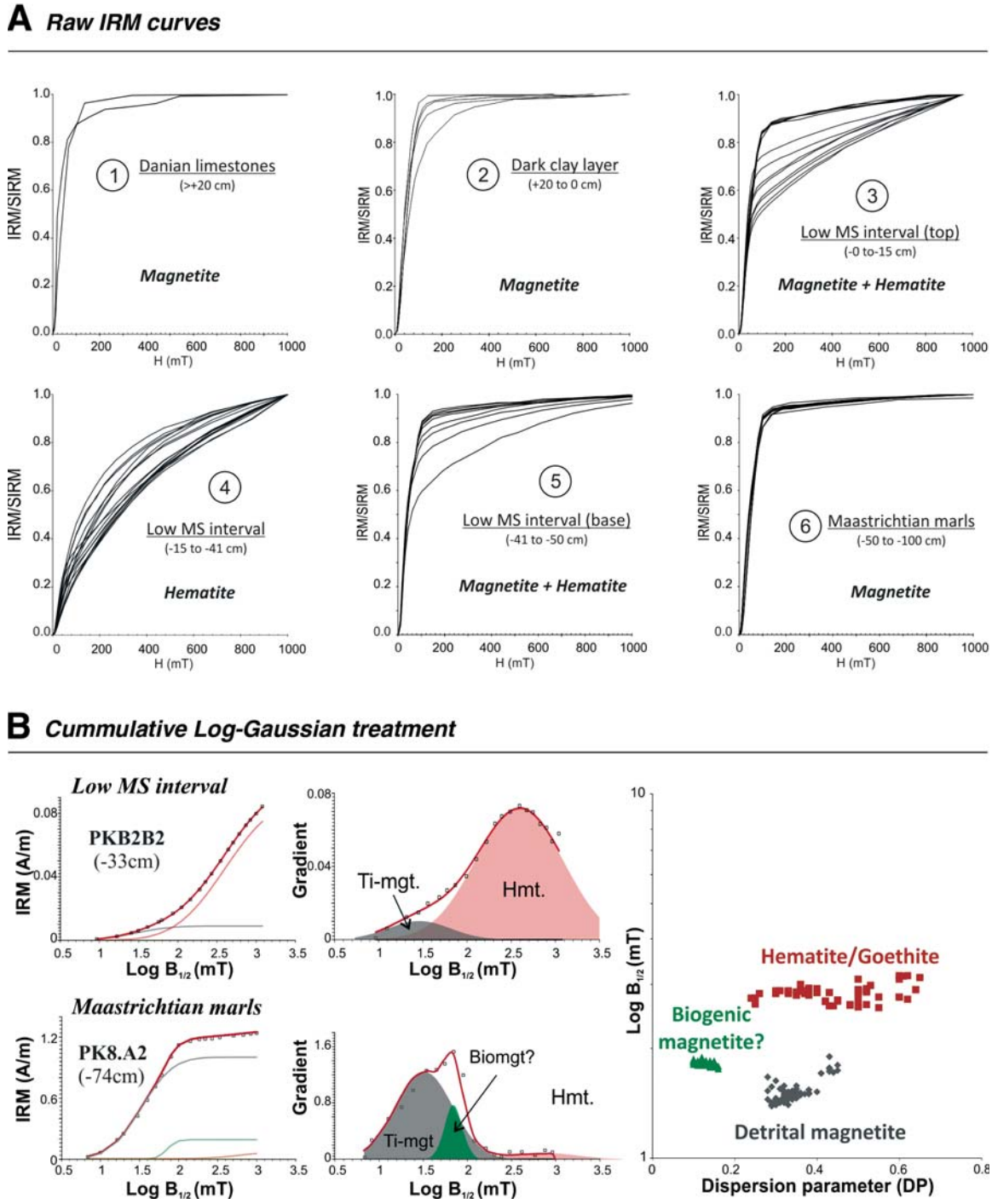

Figure 4. (A) Raw isothermal remanent magnetization (IRM; saturation isothermal remanent magnetization [SIRM]) curves of the Bidart section show that all sedimentary intervals are dominated by bimodal to trimodal distributions of remanent spectra, attributed to magnetite and hematite. (B) IRM data treated by the cumulative log-Gaussian function (Kruiver et al., 2001). In most Maastrichtian samples, component 1 (detrital magnetite) contributes to more than 90% of the magnetic signal, whereas component 2 (biomagnetite?) and component 3 (hematite) have minor contributions. The low-magnetic-susceptibility (MS) interval is characterized by very low magnetite content, disappearance of biogenic magnetite, and relative increase in hematite.

2001) and at Bidart (Galbrun and Gardin, 2004). Component 2 is observed in the whole section except in the low-MS interval, and it exhibits slightly higher coercivity (log $B_{1/2}$) and lower dispersion parameter (DP) values than component 1 (Fig. 4B). The very small dispersion of coercivity and DP parameters of component 2 (Fig. 4B) argues for the presence of a homogeneous population of the magnetic carrier in terms of grain size and composition (Egli, 2004). Such homogeneity and the very narrow distribution of component 2 (mean DP = 0.12) are usually indicative of the presence of magnetic grains (magnetosomes) produced by magnetotactic bacteria (Egli, 2004; Abrajevitch and Kodama, 2009, 2011). Values of remanent coercivity ($B_{1/2}$) of the hard fraction vary between 389 and 1479 mT and are typical of antiferromagnetic behavior, similar to hydroxides such as hematite or goethite commonly found in marine rocks (Kruiver et al., 2003). However, goethite has not been identified under thermomagnetic analysis (Font et al., 2011). Akaganeite is paramagnetic at ambient temperature (Néel temperature of 290 °K) and thus cannot be the carrier of the high-coercivity curve. Hematite is therefore likely the high-coercivity phase.

The decrease in MS values can be explained by reduced detrital titanomagnetite (and biogenic magnetite) content, the main magnetic carrier of the Maastrichtian marls at Bidart (Galbrun and Gardin, 2004; Font et al., 2011), as observed by a characteristic reduction in mass-normalized SIRM values of component 1 and 2 (Fig. 3–4). A maximum 90% reduction in component 1 + 2 remanence is observed in the middle part of the interval (Fig. 3).

SCANNING ELECTRON MICROSCOPY

We observed more than 10 samples, including the Danian and Maastrichtian sediments. SEM observations coupled to EDS show the occurrence of Cl-bearing iron hydroxides with a specular, plate-like morphology and grain sizes <10–40 µm (Fig. 5). This mineral was only observed in samples from the low-MS interval, whereas Fe-Ti iron oxides are the sole magnetic carriers in the rest of the section. EDS spectra show the presence of Fe, O, Cl, and Ca. Compositional mapping reveals only Fe and Cl together, whereas Ca is associated with the sediment matrix (Fig. 5). Ti-bearing iron oxides (Ti being an indicator of detrital origin) are rare in samples from the low-MS interval but exist either as small (<10 µm) cubic-like and eroded crystals of magnetite or as severely altered ilmenite (Fig. 6).

We infer that the Cl-rich iron hydroxide corresponds to akaganeite, in agreement with our SEM-EDS data. Concentration in Cl was estimated by semiquantitative analysis of EDS spectra (more than 20 analyses) and varies between 0.68 and 4.64 wt%, which we consider corresponds to a minimum value since other elements contained in the matrix also contribute to the calculation. The association Fe-Cl is explained by the hollandite-type structure of akaganeite (Post and Buchwald, 1991). In this arrangement, the octahedral sites are occupied by iron cations, whereas Cl^- ions partially fill the tunnels. The subeuhedral and plate-like morphologies of the crystals contrast with the eroded aspect of the detrital titanomagnetite and rather argue for an eolian transport mechanism (Fig. 6). Grain sizes from micrometer to tens of micrometers are in the range of Quaternary eolian dust (Maher, 2011). The presence of akaganeite, which strongly reflects in the yellow-brown region, is also consistent with DRS, which show significant trends in the low-MS interval in the red (CIE_a) and yellow (CIE_b) colors (Fig. 3). It also explains the characteristic yellow-brown color of the low-MS interval at Bidart (Figs. 1 and 3).

DISCUSSION

Akaganeite: A New Deccan Marker?

The discovery of akaganeite in the low-MS interval at Bidart (this study) and at Gubbio (Font et al., 2011) just below the Cretaceous-Paleogene boundary mass extinction and coeval with the main Deccan phase 2 argues for a volcanic origin. The subeuhedral and plate-like morphologies of the newly found akaganeite crystals contrast with the eroded aspect of detrital magnetite, and their scarcity (<0.1 wt%) in the sedimentary matrix is compatible with eolian transport from a distant source. Akaganeite (β-$Fe_2[OH]_3Cl$) is rare in natural conditions but a common product of corrosion of steel or archaeological items in marine environments because its formation requires large concentrations of both dissolved Fe(II) and chloride ions (Reguer et al., 2007; Remazeilles and Refait, 2007, 2008). Akaganeite is also described from weathered steel exposed to an acidic atmosphere (Li et al., 2008). Johnston (1977) described akaganeite co-occurring with jarosite near the steaming fumarole vents of the White Island volcano in New Zealand. Akaganeite also precipitates naturally as a pure mineral phase with an average Fe/Cl molar ratio of 6.7 from oxidation of iron sulfide minerals during occasional drying of sulfide sediments from Australian wetlands (Bibi et al., 2011). Naturally occurring akaganeite is also observed in weathered meteorites, especially from cold environments such as the Antarctic continent (Bland et al., 1997; Lee and Bland, 2004). Akaganeite from meteorites often contains a small amount of Ni.

Akaganeite crystals found in the Bidart and Gubbio sediments do not have the composition of meteorite-derived akaganeite. Their formation in periodically dried sulfidic coastal wetlands in the vicinity of the Deccan Traps is a possible scenario, but in this hypothesis their transportation to Gubbio (Italy) and Bidart (France) is highly unlikely (Font et al., 2011). However, their formation in relation with Deccan volcanic degassing followed by eolian transport is a possible scenario.

Metal transfer (notably Fe but also Na, K, Zn) from degassing lava to the atmosphere as simple chlorides has been observed and predicted by thermochemical modeling. These compounds are highly volatile, especially when the lava is at a high temperature. We infer that akaganeite results from a gaseous reaction between such iron chlorine compounds and volcanic/atmospheric gases, such as water and oxygen. The structural formula of akaganeite (oxyhydroxide and not oxide) pleads for a reaction at a rather

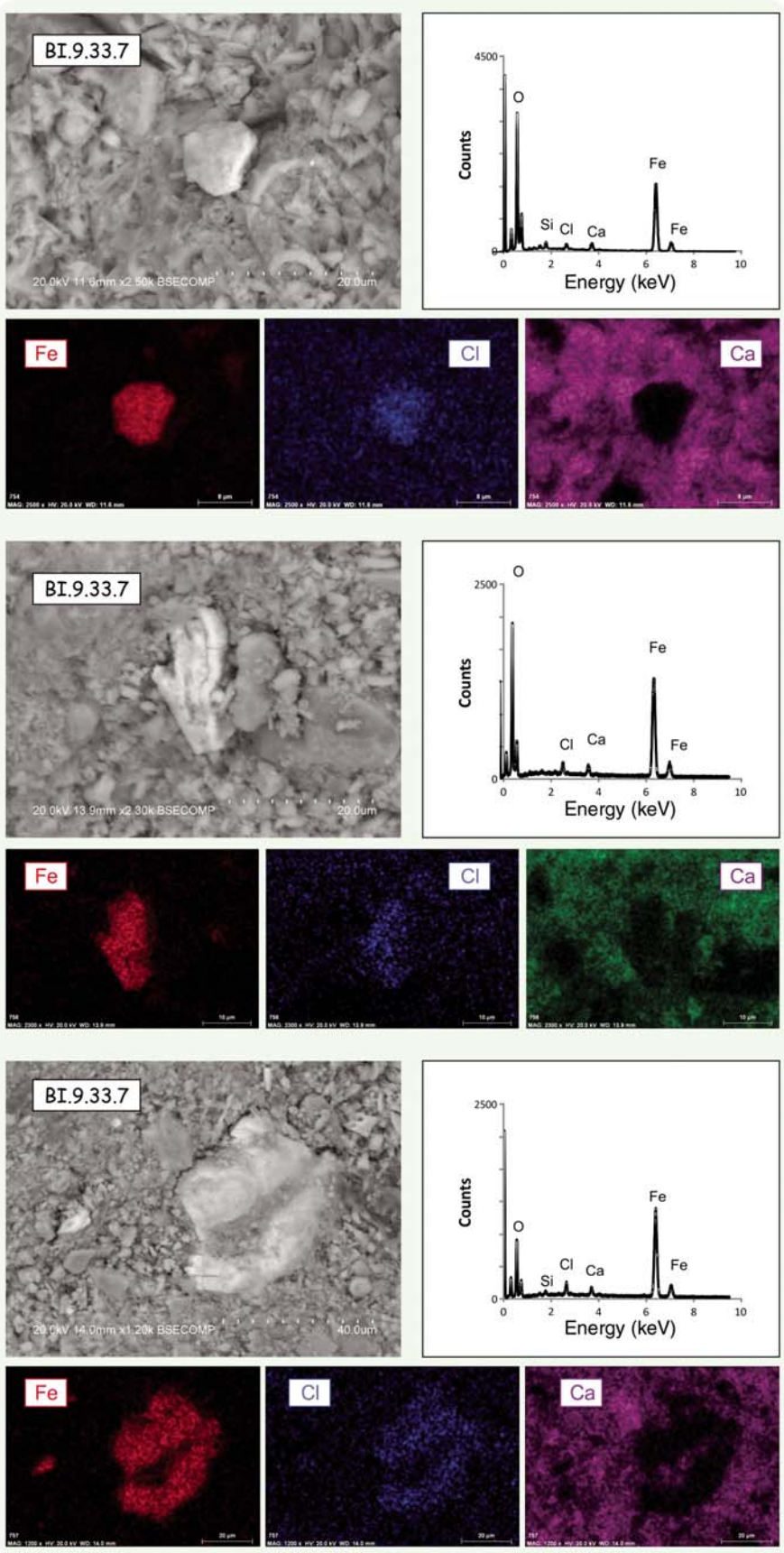

Figure 5. Scanning electron microscopy coupled to energy dispersive spectra (EDS) and composition mapping of the Cl-bearing iron hydroxide found in the interval of low-magnetic-susceptibility (MS) values at Bidart.

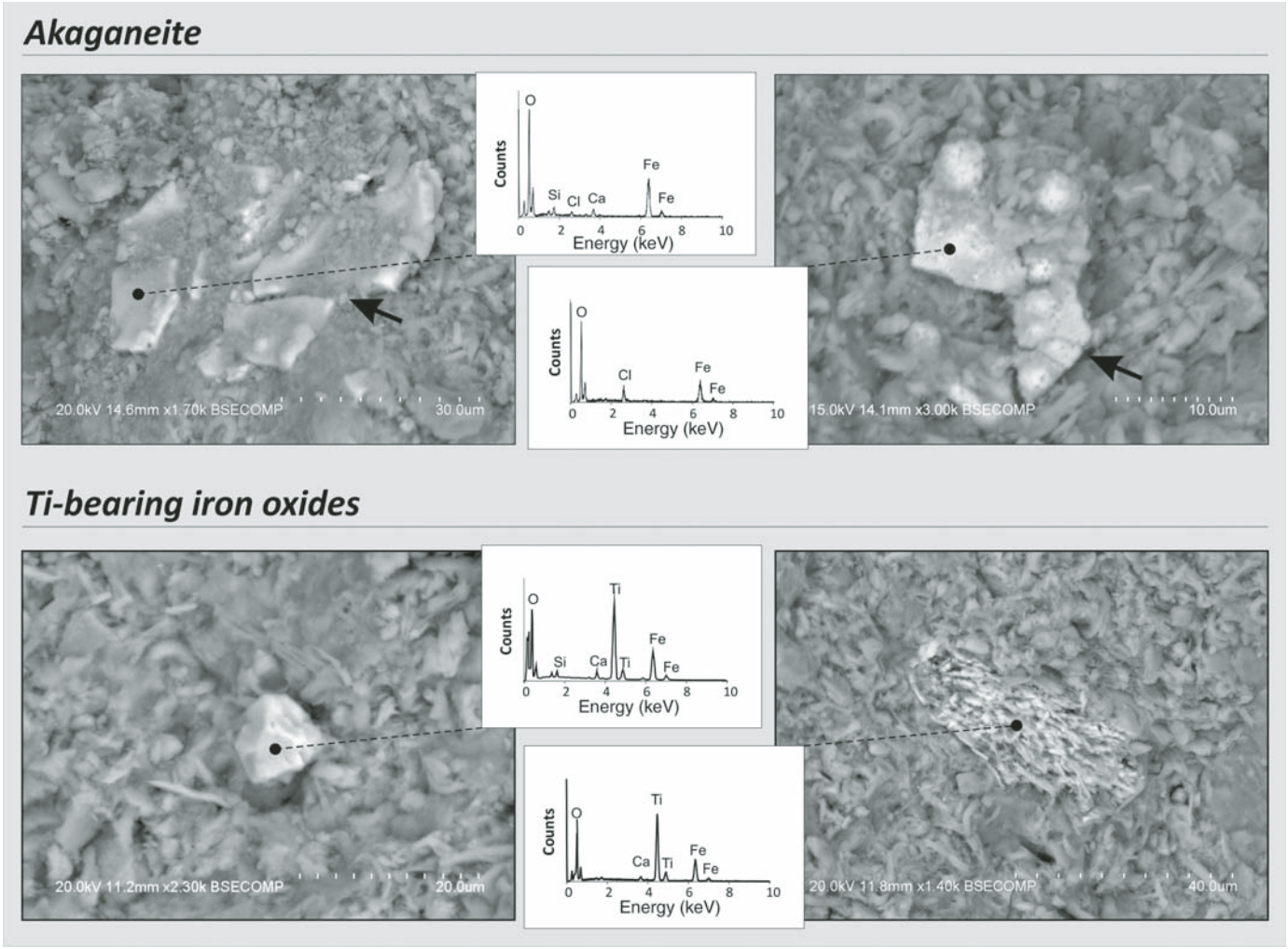

Figure 6. Additional scanning electron microscopy photographs and energy dispersive spectra (EDS) spectra of plate-like and semihexagonal akaganeite and eroded and severely altered Ti-bearing iron oxides.

low temperature. Indeed, at temperatures higher than 550 °C, akaganeite would react to form hematite. At these temperatures, $FeCl_2$ is the most abundant iron species, whereas at temperatures higher than 750 °C, it is replaced by $Fe(OH)_2$ (Symonds and Reed, 1993). $FeCl_2$ sublimates rapidly (64.4 mg/100 mL), allowing its dissolution in the aqueous and atmospheric medium. Fe^{2+} and Cl^- ions could then react according to the following equation to form akaganeite:

$$2Fe^{2+}_{(aq)} + Cl^-_{(aq)} + 3/2H_2O + 3/4O_2(g) = \beta\text{-}Fe_2(OH)_3Cl_{(s)}. \quad (3)$$

Considering a standard free energy of formation for β-$Fe_2(OH)_3Cl$ (Remazeilles and Refait, 2007) and enthalpies of aqueous Fe(II), Cl(II), and water (Wagman et al., 1982), the computed ΔG°_r is –280.74 kJ mol^{-1}. According to this reactive pathway, the akaganeite formation is thermodynamically possible.

Delivery of SO_2 and halogens to the atmosphere by active volcanoes is well known, especially for arc volcanism (Pyle and Mather, 2009), but it also occurs in continental flood basalt eruptions (Thordarson and Self, 1996; Self et al., 2008b). Glass analyses recently demonstrated that Deccan basalts were responsible for a huge HCl input into the atmosphere (4×10^{12} g SO_2 and 1×10^{12} g HCl released into the atmosphere per cubic kilometer of lava; Self et al., 2008b), confirming former scenarios (Glasby and Kunzendorf, 1996). The volume of lavas extruded during Deccan phase 2 is ~80% of the total lava volume, i.e., ~10^6 km^3 (Self et al., 2006). These figures are fairly consistent with the calculations of Black et al. (2012) for the Siberian Traps, which are suggested to have released 7×10^{12} g S and 3–9 $\times 10^{12}$ g Cl into the atmosphere. In the latter case, the variability of Cl degassing is due to the possible contribution of contact heating and metamorphism of the Tunguska sediments. The Kilauea volcano in Hawaii sometimes generates additional HCl when lavas flow into the sea (Edmonds and Gerlach, 2006). Using the conservative hypothesis of 1×10^{12} g HCl released by Deccan phase 2 for 200,000 yr, a mean value of 5 Mt Cl and 10 Mt S per year would

have been released into the atmosphere (i.e., quantities equivalent to one Pinatubo eruption every year or every 2 yr for 200,000 yr). These calculations assume a rather unrealistic regular volcanic gas production and over a much longer time period than the currently estimated tens of thousands of years to at most 50,000–100,000 yr (Chenet et al., 2008). Despite these uncertainties, it is obvious that Deccan phase 2 corresponds to a severe atmospheric change and was responsible for major environmental hazards due to acid rains over tens of thousands of years, as recently suggested by Ward (2009).

The fate of the acidic gases depends on humidity at the emission site, because of their very high water solubility. At the time of Deccan phase 2 volcanism, India was a large island in the southern part of the Tethys Ocean located at ~21°S. Climate was relatively warm and humid, but arid close to the Deccan volcanic province as a result of "mock aridity" (e.g., volcanically induced conditions and extreme geochemical alkalinity; Khadkikar et al., 1999; Gertsch et al., 2011; Keller et al., 2012). Therefore, a large proportion of the released gases would have been transported into the high atmosphere (Kaminski et al., 2011) rather than scavenged locally by rains. Deccan volcanism likely occurred as large fissure eruptions with thermal plumes penetrating into the stratosphere due to the high lava volume and high temperatures (Self et al., 2006). A significant percentage of acid gases and halogens is therefore expected to have remained in the lower stratosphere for several years after each eruption (Ward, 2009). This is the likely explanation for environmental changes such as acid rains over a large portion of Earth, especially the intertropical and peri-Tethys regions.

Low-MS Interval: Consequence of Deccan Phase 2 Acid Rains?

Low-MS values just below the Cretaceous-Paleogene boundary may reflect a drastic decrease in the main magnetite component, that is, detrital titanomagnetite (component 1), originating from erosion of igneous rocks and/or their pedogenetic products and being transported into basin sediments. Absence of biomagnetite is also observed in the low-MS interval, but its origin still needs to be confirmed in the future. Variations in detrital titanomagnetite content at Bidart can be explained by several causes, such as (1) a rapid sea-level rise (e.g., dilution and remoteness to the source), (2) diagenetic reduction (Abrajevitch and Kodama, 2011), or (3) annihilation of iron oxides at or close to their continental source. The third hypothesis is tested here as a consequence of the huge Deccan volcanic gas emissions and resulting acid rains, which could have dissolved the continental magnetite grains before any riverine transfer to the oceanic basin. Rain in equilibrium with present-day atmospheric CO_2 is characterized by a pH of 5.6, whereas acidic volcanic rains have a much lower pH. For instance, the distribution of regional rain pH due to Mount Etna, a major gas emitter, has a pH of 3–4.5 (Calabrese et al., 2011).

Our weathering model indicates that equilibrium between magnetite and the weathering solution is reached between rain events (~1 d). The time required to dissolve 90% of the initial magnetite mass is between 31,000 (pH 3.3) and 68,000 yr (pH 4.3). These values are compatible with the temporal duration of the volcanic emissions based upon magneto-stratigraphic measurements and estimated at less than 100 k.y. (10–20 yr per flow; Chenet et al., 2007, 2008). Note that our calculations based on the pH of present-day rainwater (5.6) lead to a dissolution time of several million years, which is much longer than the expected landscape Davisian stability and consistent with previous work (White et al., 1994) giving very long residence time for sand-sized grains of magnetite subjected to present-day weathering conditions.

Conceptual Model

A conceptual model for the formation of akaganeite and its eolian deposition at Bidart and Gubbio infers the formation of akaganeite in the buoyant volcanic plume and transportation into the stratosphere by penetrative convection together with huge amounts of aerosols containing dissolved acid species (Fig. 7). It is well known that heat associated with widespread lava flows may generate convection in the atmosphere (Kaminski et al., 2011). These penetrative convections produce a thick well-mixed heated atmospheric layer where buoyancy ensures that volcanic gases get transported to the stratosphere, despite the low explosive nature of tholeiitic volcanism.

Subtropical eruptions such as the Deccan Traps are important contributors to global climate because stratospheric aerosols have a long lifetime in the tropical-subtropical stratosphere and can be transported into the midlatitudes of both hemispheres. For example, in the Soufrière Hills eruption (16.7°N) in 2006, the aerosol plume reached altitudes up to 20 km (Prata et al., 2007), which is well above the tropical tropopause layer. Two weeks after the eruption of the Nabro volcano (East Africa, 13.5°N) in 2011, the Cloud Aerosol Lidar and Infrared Pathfinder Satellite Observation (CALIPSO) detected enhanced aerosol backscatter in the lower stratosphere (~18 km; Vernier et al., 2013). During the 1991 Pinatubo eruption (15°N), the plume reached a maximum altitude of 39 km (Holasek et al., 1996), whereas the buoyant regions of the volcanic SO_2 and ash cloud are estimated at 25 km and 22 km, respectively (Guo et al., 2004b).

Once injected into the stratosphere, the large aerosol particles and small ones being formed by the volcanic gases are rapidly advected around the globe (Robock, 2000). The lifetime of sulfate aerosols is up to 3 yr in the stratosphere, but only 3 wk in the troposphere. Observations after the 1883 Krakatau eruption (6°S) showed that the aerosol cloud circled the globe in 2 wk (Robock, 2000). The El Chichón (17°N) eruption in 1982 and the Pinatubo eruption in 1991 are other examples of volcanic eruptions where aerosol clouds circled the globe within 3 wk and caused considerable cooling of the lower troposphere in the 2 yr after the eruptions (Robock, 2000; Guo et al., 2004a). The effect of the Laki eruption (1783) in Iceland, which extruded ~15 km^3 of lava over 8 mo (Thordarson and Self, 2003), is also well documented,

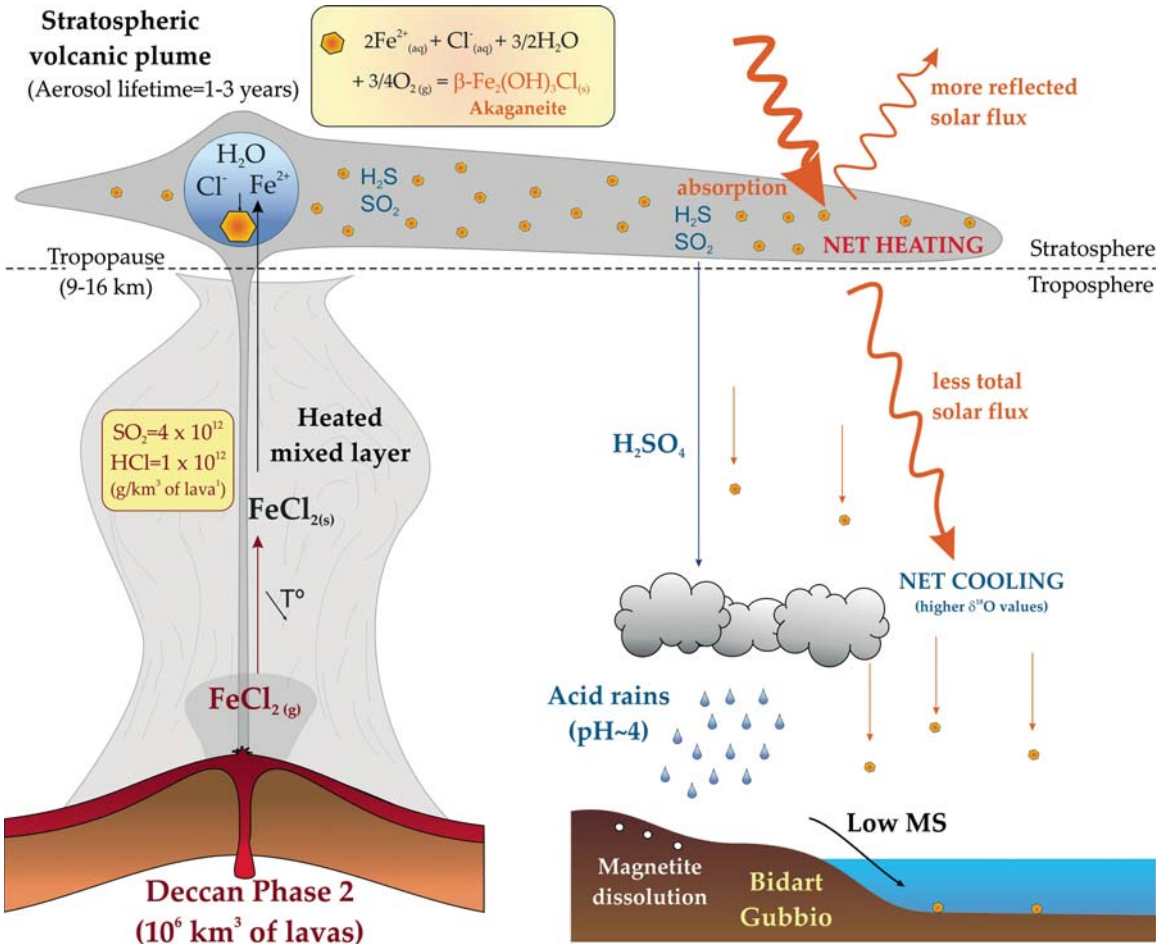

Figure 7. Conceptual model of the sedimentary marine record of continental magnetite dissolution caused by volcanic acidic rains (modified from Kaminski et al., 2011; Robock, 2000). MS—magnetic susceptibility.

including climate change and acid rains over most of Europe up to 3000 km from the volcano (Garnier, 2011). Numerical modeling of the Laki eruption confirmed that cooling was mostly due to stratospheric sulfate aerosols (Chenet et al., 2005).

In comparison, Deccan eruptions were much more intense, with an estimated 1 × 10^6 km^3 lava extruded (Self et al., 2006) over tens of thousands of years (Chenet et al., 2007). This likely caused acid rains through the intertropical peri-Tethys zone, reaching the North Atlantic and France (Bidart), in particular, ~7000 km from the erupting Deccan basalts. Our model assumes that Deccan volcanism caused acid rain at Bidart (France) and Gubbio (Italy), resulting in weathering and a dissolution effect on the continental surface. As noted earlier, these assumptions are well supported by historical comparisons, as well as our numerical weathering model. The subsequent cooling effect results from the huge input of stratospheric aerosols (Self et al., 2006, 2008b), as also supported by our carbon and oxygen isotopic data (Fig. 2).

We conclude that since volcanic plumes of relatively very small volcanic eruptions have reached the stratosphere and caused significant acid rain and climate changes over relatively very large areas (~3000 km for the Laki eruption, which extruded 15 km^3 of lava), then the giant pulsed Deccan eruptions near the end of the Maastrichtian, with an estimated 800,000 km^3 lava erupted (~53 times the Laki eruptions; Self et al., 2006), must have resulted in the most devastating global environmental changes. A comparison of stratospheric volcanic aerosol output from recent volcanos and its effect on Earth's radiation budget with the output from Deccan eruptions reveals further clues to the magnitude, nature, and importance of the enormous global Deccan-related environmental changes and their likely devastating contribution to the end-Cretaceous mass extinction.

CONCLUSION

The magnetic and mineral markers identified in the Bidart section are consistent with a major change in atmospheric conditions linked to Deccan-induced volcanic gas emissions. The low-MS signal is likely to be recognized elsewhere in the

Tethys sedimentary record, particularly in shallow and proximal marine environments where terrestrial input is appropriate and provided that wet local climatic conditions prevailed and that the continental surfaces contained significant amounts of magnetite. Presence of akaganeite is expected in the Tethys realm, but with a variable probability depending on the mechanisms of eolian transport. Moreover, both markers may help unravel the signature of other large igneous provinces emplaced in similar paleogeographic and paleoclimatic conditions, such as the Central Atlantic magmatic province. These newly discovered markers provide a promising tool with which to evaluate the environmental effects of large igneous provinces and their possible consequences for the biosphere.

ACKNOWLEDGMENTS

Funding was provided by Fundação para a Ciências e a Tecnologia (PTDC/CTE_GIX/110205/2010). We thank Celia Lee and Ana Sousa for technical and administrative supply, Bernard Peybernès for bibliographic supply and help in the field, and Dominique Serça and Céline Mari (Laboratoire d'Aérologie, Observatoire Midi-Pyrénées, Toulouse), Gilles Berger (IRAP, Institut de Recherche en Astrophysique et Planétologie, Toulouse), and Alexandra Abrajevitch (Institute of Tectonics and Geophysics, Russian Academy of Sciences, Khabarovsk) for helpful discussions. We thank anonymous reviewers for their constructive comments.

REFERENCES CITED

Abrajevitch, A., and Kodama, K., 2009, Biochemical vs. detrital mechanism of remanence acquisition in marine carbonates: A lesson from the K-T boundary interval: Earth and Planetary Science Letters, v. 286, p. 269–277, doi:10.1016/j.epsl.2009.06.035.

Abrajevitch, A., and Kodama, K., 2011, Diagenetic sensitivity of paleoenvironmental proxies: A rock magnetic study of Australian continental margin sediments: Geochemistry Geophysics Geosystems, v. 12, p. 1–18, doi:10.1029/2010GC003481.

Abramovich, S., Yovel-Corem, S., Almogi-Labin, A., and Benjamini, C., 2010, Global climate change and planktic foraminiferal response in the Maastrichtian: Paleoceanography, v. 25, p. PA2201, doi:10.1029/2009PA001843.

Bibi, I., Singh, B., and Silvester, E., 2011, Akaganeite (beta-FeOOH) precipitation in inland acid sulfate soils of south-western New South Wales (NSW), Australia: Geochimica et Cosmochimica Acta, v. 75, p. 6429–6438, doi:10.1016/j.gca.2011.08.019.

Black, B.A., Elkins-Tanton, L.T., Rowe, M.C., and Peate, I.U., 2012, Magnitude and consequences of volatile release from the Siberian Traps: Earth and Planetary Science Letters, v. 317, p. 363–373, doi:10.1016/j.epsl.2011.12.001.

Bland, P.A., Kelley, S.P., Berry, F.J., Cadogan, J.M., and Pillinger, C.T., 1997, Artificial weathering of the ordinary chondrite Allegan: Implications for the presence of Cl^- as a structural component in akaganeite: The American Mineralogist, v. 82, p. 1187–1197.

Bonté, P., Delacotte, O., Renard, M., Laj, C., Boclet, D., Jehanno, C., and Rocchia, R., 1984, An iridium-rich layer at the Cretaceous-Tertiary boundary in the Bidart section (southern France): Geophysical Research Letters, v. 11, p. 473–476, doi:10.1029/GL011i005p00473.

Brunauer, S., Emmett, P.H., and Teller, E., 1938, Adsorption of gases in multimolecular layers: Journal of the American Chemical Society, v. 60, p. 309–319, doi:10.1021/ja01269a023.

Calabrese, S., Aiuppa, A., Allard, P., Bagnato, E., Bellomo, S., Brusca, L., D'Alessandro, W., and Parello, F., 2011, Atmospheric sources and sinks of volcanogenic elements in a basaltic volcano (Etna, Italy): Geochimica et Cosmochimica Acta, v. 75, p. 7401–7425, doi:10.1016/j.gca.2011.09.040.

Channell, J.E.T., Hodell, D.A., Singer, B.S., and Xuan, C., 2010, Reconciling astrochronological and Ar-40/Ar-39 ages for the Matuyama-Brunhes boundary and late Matuyama chron: Geochemistry Geophysics Geosystems, v. 11, p. Q0AA12, doi:10.1029/2010GC003203.

Chenet, A.L., Fluteau, F., and Courtillot, V., 2005, Modelling massive sulphate aerosol pollution, following the large 1783 Laki basaltic eruption: Earth and Planetary Science Letters, v. 236, p. 721–731, doi:10.1016/j.epsl.2005.04.046.

Chenet, A.L., Quidelleur, X., Fluteau, F., Courtillot, V., and Bajpai, S., 2007, K-40-Ar-40 dating of the Main Deccan large igneous province: Further evidence of KTB age and short duration: Earth and Planetary Science Letters, v. 263, p. 1–15, doi:10.1016/j.epsl.2007.07.011.

Chenet, A.L., Fluteau, F., Courtillot, V., Gerard, M., and Subbarao, K.V., 2008, Determination of rapid Deccan eruptions across the Cretaceous-Tertiary boundary using paleomagnetic secular variation: Results from a 1200-m-thick section in the Mahabaleshwar escarpment: Journal of Geophysical Research–Solid Earth, v. 113, p. B04101, doi:10.1029/2006JB004635.

Chudaeva, V.A., Urchenko, S.G., Chudaev, O.V., Sugimory, K., Matsuo, M., and Kuno, A., 2006, Chemistry of rainwaters in the south Pacific area of Russia: Journal of Geochemical Exploration, v. 88, p. 101–105, doi:10.1016/j.gexplo.2005.08.020.

Commission Internationale de L'Eclairage (CIE), 1978, Recommendations on uniform color spaces, color difference equations, psychometric color terms: Supplement No 2 to Publication 15, Colorimetry: Paris, Bureau Central de la CIE.

Courtillot, V., 2012, Mass extinctions and massive volcanism: Journal of the Geological Society of India, v. 79, p. 107–108.

Edmonds, M., and Gerlach, T.M., 2006, The airborne lava-seawater interaction plume at Kilauea volcano, Hawai'i: Earth and Planetary Science Letters, v. 244, p. 83–96, doi:10.1016/j.epsl.2006.02.005.

Egli, R., 2004, Characterization of individual rock magnetic components by analysis of remanence curves: 1. Unmixing natural sediments: Studia Geophysica et Geodaetica, v. 48, p. 391–446, doi:10.1023/B:SGEG.0000020839.45304.6d.

Ellwood, B.B., MacDonald, W.D., Wheeler, C., and Benoist, S.L., 2003, The K-T boundary in Oman: Identified using magnetic susceptibility field measurements with geochemical confirmation: Earth and Planetary Science Letters, v. 206, p. 529–540, doi:10.1016/S0012-821X(02)01124-X.

Fabre, S., and Berger, G., 2012, How tillite weathering during the snowball Earth aftermath induced cap carbonate deposition: Geology, v. 40, p. 1027–1030, doi:10.1130/G33340.1.

Fabre, S., Berger, G., and Nedelec, A., 2011, Modeling of continental weathering under high-CO_2 atmospheres during Precambrian times: Geochemistry Geophysics Geosystems, v. 12, p. Q10001, doi:10.1029/2010GC003444.

Floor, G.H., Calabrese, S., Roman-Ross, G., D'Alessandro, W., and Aiuppa, A., 2011, Selenium mobilization in soils due to volcanic derived acid rain: An example from Mt. Etna volcano, Sicily: Chemical Geology, v. 289, p. 235–244, doi:10.1016/j.chemgeo.2011.08.004.

Font, E., Nedelec, A., Ellwood, B.B., Mirao, J., and Silva, P.F., 2011, A new sedimentary benchmark for the Deccan Traps volcanism?: Geophysical Research Letters, v. 38, p. L24309, doi:10.1029/2011GL049824.

Gaillardet, J., Dupre, B., Louvat, P., and Allegre, C.J., 1999, Global silicate weathering and CO_2 consumption rates deduced from the chemistry of large rivers: Chemical Geology, v. 159, p. 3–30, doi:10.1016/S0009-2541(99)00031-5.

Galbrun, B., and Gardin, S., 2004, New chronostratigraphy of the Cretaceous-Paleogene boundary interval at Bidart (France): Earth and Planetary Science Letters, v. 224, p. 19–32, doi:10.1016/j.epsl.2004.04.043.

Garnier, E., 2011, Les brouillards du Laki en 1783: Volcanisme et crise sanitaire en Europe: Bulletin de l'Académie Nationale de Médecine, v. 195, p. 1043–1055.

Gertsch, B., Keller, G., Adatte, T., Garg, R., Prasad, V., Berner, Z., and Fleitmann, D., 2011, Environmental effects of Deccan volcanism across the Cretaceous-Tertiary transition in Meghalaya, India: Earth and Planetary Science Letters, v. 310, p. 272–285, doi:10.1016/j.epsl.2011.08.015.

Glasby, G.P., and Kunzendorf, H., 1996, Multiple factors in the origin of the Cretaceous/Tertiary boundary: The role of environmental stress and Deccan Trap volcanism: Geologische Rundschau, v. 85, p. 191–210, doi:10.1007/BF02422228.

Guo, S., Bluth, G.J.S., Rose, W.I., Watson, I.M., and Prata, A.J., 2004a, Re-evaluation of SO_2 release of the 15 June 1991 Pinatubo eruption using ultraviolet and infrared satellite sensors: Geochemistry Geophysics Geosystems, v. 5, p. Q04001, doi:10.1029/2003GC000654.

Guo, S., Rose, W.I., Bluth, G.J.S., and Watson, I.M., 2004b, Particles in the great Pinatubo volcanic cloud of June 1991: The role of ice: Geochemistry Geophysics Geosystems, v. 5, p. Q05003, doi:10.1029/2003GC000655.

Holasek, R.E., Self, S., and Woods, A.W., 1996, Satellite observations and interpretation of the 1991 Mount Pinatubo eruption plumes: Journal of Geophysical Research–Solid Earth, v. 101, p. 27,635–27,655, doi:10.1029/96JB01179.

Johnston, J.H., 1977, Jarosite and akaganeite from White Island volcano, New Zealand—An X-ray and Mossbauer study: Geochimica et Cosmochimica Acta, v. 41, p. 539–544, doi:10.1016/0016-7037(77)90291-5.

Kaminski, E., Chenet, A.L., Jaupart, C., and Courtillot, V., 2011, Rise of volcanic plumes to the stratosphere aided by penetrative convection above large lava flows: Earth and Planetary Science Letters, v. 301, p. 171–178, doi:10.1016/j.epsl.2010.10.037.

Keller, G., Li, L., and MacLeod, N., 1995, The Cretaceous-Tertiary boundary stratotype section at El Kef, Tunisia: How catastrophic was the mass extinction?: Palaeogeography, Palaeoclimatology, Palaeoecology, v. 119, p. 221–254, doi:10.1016/0031-0182(95)00009-7.

Keller, G., Adatte, T., Gardin, S., Bartolini, A., and Bajpai, S., 2008, Main Deccan volcanism phase ends at K-T mass extinction: Evidence from the Krishna-Godavari Basin, SE India: Earth and Planetary Science Letters, v. 268, p. 293–311.

Keller, G., Adatte, T., Juez, A.P., and Lopez-Oliva, J.G., 2009, New evidence concerning the age and biotic effects of the Chicxulub impact in NE Mexico: Journal of the Geological Society, v. 166, p. 393–411, doi:10.1144/0016-76492008-116.

Keller, G., Bhowmick, P.K., Upadhyay, H., Dave, A., Reddy, A.N., Jaiprakash, B.C., and Adatte, T., 2011, Deccan volcanism linked to the Cretaceous-Tertiary boundary mass extinction: New evidence from ONGC wells in the Krishna-Godavari Basin: Journal of the Geological Society of India, v. 78, p. 399–428, doi:10.1007/s12594-011-0107-3.

Keller, G., Adatte, T., Bhowmick, P.K., Upadhyay, H., Dave, A., Reddy, A.N., and Jaiprakash, B.C., 2012, Nature and timing of extinctions in Cretaceous-Tertiary planktic foraminifera preserved in Deccan intertrappean sediments of the Krishna–Godavari Basin, India: Earth and Planetary Science Letters, v. 341–344, p. 211–221, doi:10.1016/j.epsl.2012.06.021.

Khadkikar, A.S., Sant, D.A., Gogte, V., and Karanth, R.V., 1999, The influence of Deccan volcanism on climate: Insights from lacustrine intertrappean deposits, Anjar, western India: Palaeogeography, Palaeoclimatology, Palaeoecology, v. 147, p. 141–149, doi:10.1016/S0031-0182(98)00156-4.

Kruiver, P.P., Dekkers, M.J., and Heslop, D., 2001, Quantification of magnetic coercivity components by the analysis of acquisition curves of isothermal remanent magnetisation: Earth and Planetary Science Letters, v. 189, p. 269–276, doi:10.1016/S0012-821X(01)00367-3.

Kruiver, P.P., Langereis, C.G., Dekkers, M.J., and Krijgsman, W., 2003, Rock-magnetic properties of multicomponent natural remanent magnetization in alluvial red beds (NE Spain): Geophysical Journal International, v. 153, p. 317–332, doi:10.1046/j.1365-246X.2003.01880.x.

Kuiper, K.F., Deino, A., Hilgen, F.J., Krijgsman, W., Renne, P.R., and Wijbrans, J.R., 2008, Synchronizing rock clocks of Earth history: Science, v. 320, p. 500–504, doi:10.1126/science.1154339.

Lee, M.R., and Bland, P.A., 2004, Mechanisms of weathering of meteorites recovered from hot and cold deserts and the formation of phyllosilicates: Geochimica et Cosmochimica Acta, v. 68, p. 893–916, doi:10.1016/S0016-7037(03)00486-1.

Li, L.Q., and Keller, G., 1998, Abrupt deep-sea warming at the end of the Cretaceous: Geology, v. 26, p. 995–998, doi:10.1130/0091-7613(1998)026<0995:ADSWAT>2.3.CO;2.

Li, Q.X., Wang, Z.Y., Han, W., and Han, E.H., 2008, Characterization of the rust formed on weathering steel exposed to Qinghai salt lake atmosphere: Corrosion Science, v. 50, p. 365–371, doi:10.1016/j.corsci.2007.06.020.

Maher, B.A., 2011, The magnetic properties of Quaternary aeolian dusts and sediments, and their palaeoclimatic significance: Aeolian Research, v. 3, p. 87–144, doi:10.1016/j.aeolia.2011.01.005.

Pardo, A., Ortiz, M., and Keller, G., 1996, Latest Maastrichtian and Cretaceous-Tertiary boundary foraminiferal turnover and environmental changes at Agost, Spain, *in* MacLeod, N., and Keller, G., eds., Cretaceous-Tertiary Mass Extinction: Biotic and Environmental Changes: New York, W.W. Norton and Company, p. 139–171.

Parkhurst, D.L., and Appelo, C.A.J., 1999. User's Guide to PHREEQC Version 2—A Computer Program for Speciation, Batch-Reaction, One-Dimensional Transport, and Inverse Calculations: U.S. Geological Survey Water-Resources Investigations Report 99-4259, 312 p.

Post, J.E., and Buchwald, V.F., 1991, Crystal-structure refinement of akaganeite: The American Mineralogist, v. 76, p. 272–277.

Prata, A.J., Carn, S.A., Stohl, A., and Kerkmann, J., 2007, Long range transport and fate of a stratospheric volcanic cloud from Soufriere Hills volcano, Montserrat: Atmospheric Chemistry and Physics, v. 7, p. 5093–5103, doi:10.5194/acp-7-5093-2007.

Pyle, D.M., and Mather, T.A., 2009, Halogens in igneous processes and their fluxes to the atmosphere and oceans from volcanic activity: A review: Chemical Geology, v. 263, p. 110–121, doi:10.1016/j.chemgeo.2008.11.013.

Reguer, S., Dillmann, P., and Mirambet, F., 2007, Buried iron archaeological artefacts: Corrosion mechanisms related to the presence of Cl-containing phases: Corrosion Science, v. 49, p. 2726–2744, doi:10.1016/j.corsci.2006.11.009.

Remazeilles, C., and Refait, P., 2007, On the formation of beta-FeOOH (akaganeite) in chloride-containing environments: Corrosion Science, v. 49, p. 844–857, doi:10.1016/j.corsci.2006.06.003.

Remazeilles, C., and Refait, P., 2008, Formation, fast oxidation and thermodynamic data of Fe(II) hydroxychlorides: Corrosion Science, v. 50, p. 856–864, doi:10.1016/j.corsci.2007.08.017.

Renne, P.R., Mundil, R., Balco, G., Min, K.W., and Ludwig, K.R., 2010, Joint determination of K-40 decay constants and Ar-40*/K-40 for the Fish Canyon sanidine standard, and improved accuracy for Ar-40/Ar-39 geochronology: Geochimica et Cosmochimica Acta, v. 74, p. 5349–5367, doi:10.1016/j.gca.2010.06.017.

Renne, P.R., Deino, A.L., Hilgen, F.J., Kuiper, K.F., Mark, D.F., Mitchell, W.S., Morgan, L.E., Mundil, R., and Smit, J., 2013, Time scales of critical events around the Cretaceous-Paleogene boundary: Science, v. 339, p. 684–687, doi:10.1126/science.1230492.

Robertson, D.J., and France, D.E., 1994, Discrimination of remanence-carrying minerals in mixtures, using isothermal remanent magnetization acquisition curves: Physics of the Earth and Planetary Interiors, v. 82, p. 223–234, doi:10.1016/0031-9201(94)90074-4.

Robock, A., 2000, Volcanic eruptions and climate: Reviews of Geophysics, v. 38, p. 191–219, doi:10.1029/1998RG000054.

Schulte, P., Alegret, L., Arenillas, I., Arz, J.A., Barton, P.J., Bown, P.R., Bralower, T.J., Christeson, G.L., Claeys, P., Cockell, C.S., Collins, G.S., Deutsch, A., Goldin, T.J., Goto, K., Grajales-Nishimura, J.M., Grieve, R.A.F., Gulick, S.P.S., Johnson, K.R., Kiessling, W., Koeberl, C., Kring, D.A., MacLeod, K.G., Matsui, T., Melosh, J., Montanari, A., Morgan, J.V., Neal, C.R., Nichols, D.J., Norris, R.D., Pierazzo, E., Ravizza, G., Rebolledo-Vieyra, M., Reimold, W.U., Robin, E., Salge, T., Speijer, R.P., Sweet, A.R., Urrutia-Fucugauchi, J., Vajda, V., Whalen, M.T., and Willumsen, P.S., 2010, The Chicxulub asteroid impact and mass extinction at the Cretaceous-Paleogene boundary: Science, v. 327, p. 1214–1218, doi:10.1126/science.1177265.

Self, S., Widdowson, M., Thordarson, T., and Jay, A.E., 2006, Volatile fluxes during flood basalt eruptions and potential effects on the global environment: A Deccan perspective: Earth and Planetary Science Letters, v. 248, p. 518–532, doi:10.1016/j.epsl.2006.05.041.

Self, S., Jay, A.E., Widdowson, M., and Keszthelyi, L.P., 2008a, Correlation of the Deccan and Rajahmundry Trap lavas: Are these the longest and largest lava flows on Earth?: Journal of Volcanology and Geothermal Research, v. 172, p. 3–19, doi:10.1016/j.jvolgeores.2006.11.012.

Self, S., Blake, S., Sharma, K., Widdowson, M., and Sephton, S., 2008b, Sulfur and chlorine in Late Cretaceous Deccan magmas and eruptive gas release: Science, v. 319, p. 1654–1657, doi:10.1126/science.1152830.

Smit, J., 1990, Meteorite impact, extinctions and the Cretaceous-Tertiary boundary: Geologie en Mijnbouw, v. 69, p. 187–204.

Stuben, D., Kramar, U., Berner, Z.A., Meudt, M., Keller, G., Abramovich, S., Adatte, T., Hambach, U., and Stinnesbeck, W., 2003, Late Maastrichtian paleoclimatic and paleoceanographic changes inferred from Sr/Ca ratio and stable isotopes: Palaeogeography, Palaeoclimatology, Palaeoecology, v. 199, p. 107–127, doi:10.1016/S0031-0182(03)00499-1.

Sverdrup, H., and Warfvinge, P., 1995, Estimating field weathering rates using laboratory kinetics: Reviews in Mineralogy, v. 31, p. 485–541.

Symonds, R.B., and Reed, M.H., 1993, Calculation of multicomponent chemical-equilibria in gas-solid-liquid systems—Calculation methods, thermochemical data, and applications to studies of high-temperature volcanic gases with examples from Mount St-Helens: American Journal of Science, v. 293, p. 758–864, doi:10.2475/ajs.293.8.758.

Thordarson, T., and Self, S., 1996, Sulfur, chlorine and fluorine degassing and atmospheric loading by the Roza eruption, Columbia River Basalt Group, Washington, USA: Journal of Volcanology and Geothermal Research, v. 74, p. 49–73, doi:10.1016/S0377-0273(96)00054-6.

Thordarson, T., and Self, S., 2003, Atmospheric and environmental effects of the 1783–1784 Laki eruption: A review and reassessment: Journal of Geophysical Research–Atmospheres, v. 108, p. AAC 7-1–AAC 7-29.

Vernier, J.P., Thomason, L.W., Fairlie, T.D., Minnis, P., Palikonda, R., and Bedka, K.M., 2013, Comment on "Large volcanic aerosol load in the stratosphere linked to Asian monsoon transport": Science, v. 339, p. 347.

Vonhof, H.B., and Smit, J., 1997, High-resolution late Maastrichtian–early Danian oceanic Sr-87/Sr-86 record: Implications for Cretaceous-Tertiary boundary events: Geology, v. 25, p. 347–350, doi:10.1130/0091-7613(1997)025<0347:HRLMED>2.3.CO;2.

Wagman, D.D., Evans, W.H., Parker, V.B., Schumm, R.H., Halow, I., Bailey, S.M., Churney, K.L., and Nuttall, R.L., 1982, The NBS Tables of Chemical Thermodynamic Properties—Selected Values for Inorganic and C_1 and C_2 Organic Substances in SI Units: Journal of Physical and Chemical Reference Data, v. 11, p. 1.

Ward, P.D., and Kennedy, W.J., 1993, Maastrichtian ammonites from the Biscay region (France, Spain): Journal of Paleontology, v. 67, p. 1–58.

Ward, P.L., 2009, Sulfur dioxide initiates global climate change in four ways: Thin Solid Films, v. 517, p. 3188–3203, doi:10.1016/j.tsf.2009.01.005.

White, A.F., Peterson, M.L., and Hochella, M.F., 1994, Electrochemistry and dissolution kinetics of magnetite and ilmenite: Geochimica et Cosmochimica Acta, v. 58, p. 1859–1875, doi:10.1016/0016-7037(94)90420-0.

White, R.V., and Saunders, A.D., 2005, Volcanism, impact and mass extinctions: Incredible or credible coincidences?: Lithos, v. 79, p. 299–316, doi:10.1016/j.lithos.2004.09.016.

Wilf, P., Johnson, K.R., and Huber, B.T., 2003, Correlated terrestrial and marine evidence for global climate changes before mass extinction at the Cretaceous-Paleogene boundary: Proceedings of the National Academy of Sciences of the United States of America, v. 100, p. 599–604, doi:10.1073/pnas.0234701100.

Manuscript Accepted by the Society 31 January 2014

Printed in the USA